CARBON 48 (2010) 3079–3090

available at www.sciencedirect.com

ScienceDirect

journal homepage: www.elsevier.com/locate/carbon

Highly hydroxylated carbon fibres as electrode materials of all-vanadium redox flow battery

Lu Yue [a], *Weishan Li* [a,b,*], *Fengqiang Sun* [a,b], *Lingzhi Zhao* [a], *Lidan Xing* [a]

[a] *School of Chemistry and Environment, South China Normal University, Guangzhou 510006, China*
[b] *Key Lab of Electrochemical Technology on Energy Storage and Power Generation of Guangdong Higher Education Institutes, South China Normal University, Guangzhou 510006, China*

ARTICLE INFO

Article history:
Received 18 September 2009
Accepted 25 April 2010
Available online 21 May 2010

ABSTRACT

A highly effective hydroxylated-functionalization of carbon fibres for use as electrodes of all-vanadium redox flow battery (VRFB) was developed. Carbon paper made of carbon fibres was hydroxylated ultrasonically with mixed acids (H_2SO_4/HNO_3, $V_{H_2SO_4}/V_{HNO_3}$ = 3/1) in a Teflon-lined stainless steel autoclave for different time at 80 °C. The structure, composition, and electrochemical properties of the treated samples for positive and negative electrodes of VRFB were characterized with Fourier transformation infrared spectroscopy, thermogravimetric analysis, X-ray photoelectron spectrometry, scanning electron microscopy, X-ray diffraction, cyclic voltammetry, electrochemical impedance spectroscopy, and cell charge and discharge tests. The content of hydroxyl group changes from 3.8% for the untreated sample to 14.3% for the carbon paper treated in mixed acids for 10 h. The highly hydroxylated sample shows its high activity toward the redox reactions of V(II)/V(III) and V(IV)/V(V). The VRFB using the carbon paper treated for 8 h as the electrodes exhibits excellent performance under a current density of 10 mA cm^{-2}. The average voltage efficiency reaches 91.3%, and the average energy efficiency reaches 75.1%. The mechanisms for the high hydroxylation of the carbon fibres with the mixed acids and the high activity of the treated sample toward the vanadium redoxs are discussed.

1. Introduction

All-vanadium redox flow battery (VRFB) is believed to be one of important energy storage technologies, because it has many advantages, including long cycle life, high energy efficiency, separated battery capacity, low cost of maintenance, and environmental friendship [1–5]. The redox couples, V(II)/V(III) and V(IV)/V(V), as the negative and positive half-cells of VRFB, respectively, provide VRFB with an open-circuit voltage of approximately 1.2 V at 100% state of charge [6]:

$$VO^{2+} + H_2O - e^- \underset{\text{Discharge}}{\overset{\text{Charge}}{\rightleftarrows}} VO_2^+ + 2H^+,$$

$$E^0 = +1.00\ \text{V (vs. standard hydrogen electrode(SHE))}$$

$$V^{3+} + e^- \underset{\text{Discharge}}{\overset{\text{Charge}}{\rightleftarrows}} V^{2+},\ E^0 = -0.26\ \text{V (vs. SHE)}$$

Since sulfuric acid solution is used as the support electrolyte in VRFB, carbon materials, especially the polyacrylonitrile-based carbon fibres, are preferably chosen as the electrodes because of their great specific surface area, high

* *Corresponding author at:* School of Chemistry and Environment, South China Normal University, Guangzhou 510006, China. Fax: +86 20 39310256.
E-mail address: liwsh@scnu.edu.cn (W. Li).
0008-6223/$ - see front matter © 2010 Elsevier Ltd. All rights reserved.
doi:10.1016/j.carbon.2010.04.044

strength and broad potential window [7]. However, the poor electrochemical activity of carbon materials limits their widespread use in VRFB [8].

In recent years, there have been considerable interests in the improvement of electrochemical properties of carbon materials through chemical modification including the surface oxidation and surface functionalization [9–12], which involves the introduction of oxygen-containing groups such as hydroxyl (—OH), carbonyl and carboxyl. Due to the capability of converting to a variety of organic functional groups and providing active sites for electron transfer, the —OH group should be an useful precursor and functional group for the surface modification of carbon materials [13,14].

Several successful hydroxylated-functionalization processes for carbon materials have been reported recently. Chen et al. carried out the reaction of carbanion-bearing single-walled carbon nanotube (SWCNT) with epoxy ethane and successfully obtained hydroxyethylated SWCNT [15]. Tian et al. reported an electrophilic addition reaction for the functionalization of SWCNT using alcohols by microwave irradiation to prepare the hydroxylated SWCNT [16]. Due to the chemical reaction, these processes are difficult to control and involve multi-step aftertreatment, and thus are hard to enlarge from milligram scale to gram level. Pan et al. used potassium hydroxide to treat SWCNT through a solid-phase mechanochemical reaction involving a milling ball and a high-frequency shaking processes and a 14.90% content of —OH groups was obtained [17]. However, the milling ball process damages the structure of carbon materials.

Due to the low-cost, controllable oxidation degree, effective oxidation and simple reaction steps, liquid phase oxidation with concentrated acids such as sulfuric acid and nitric acid have been widely used for the functionalization of carbon materials [18–21]. However, after oxidation treatment, not only —OH groups, but also other oxygen-containing groups such as carbonyl and carboxyl, can be formed on the surface of carbon materials. Wu et al. used the concentrated (70%) nitric acid at 115 °C to treat the polyacrylonitrile-based carbon fibres and obtained the functionalized carbon fibres containing mainly carboxylic acid groups [22]. Pittman et al. reported the similar results [23]. Sun et al. used boiling concentrated H_2SO_4 to treat polyacrylonitrile-based carbon fibres for 5 h and found that more —OH groups than carbonyl groups were introduced onto carbon fibres [24]. These results suggest that the type and the content of oxygen-containing groups can be controlled by using the proper oxidants and reaction conditions [25,26].

In this study, we developed a new treatment with mixed acid (H_2SO_4/HNO_3) in a Teflon-lined stainless steel autoclave under ultrasonication, for highly effective and fast hydroxylation of carbon fibres. The treated samples were characterized by using Fourier transformation infrared spectroscopy (FTIR), X-ray photoelectron spectrometry (XPS) and thermogravimetric analysis (TGA). It is found that the —OH groups can be successfully introduced onto the surface of carbon fibres after the treatment with the mixed acid. The characterizations of electrochemical activities of the hydroxylated carbon fibres toward the redox reactions of V(II)/V(III) and V(IV)/V(V) indicate that the highly hydroxylated carbon fibres show high catalytic activity.

2. Experimental

2.1. Materials

In this experiment, the porous carbon paper (TGP-H-060) made of polyacrylonitrile-based carbon fibres was used, since it has higher mechanical strength, better electronic conductivity and larger specific surface than other carbon materials. This carbon paper with a thickness of 0.19 mm was purchased from YiBang New Power Sources Technology Co. Ltd., Japan. V_2O_5 (>99.7%) was purchased from Hunan Nanhua Chemicals Co. Ltd., China. $VOSO_4{\cdot}3H_2O$ (>99%) was purchased from Sigma–Aldrich Co. Ltd., USA. About 98% (wt%) H_2SO_4 and 70% (wt%) HNO_3 were purchased from Shanghai Shenxiang Chemical Reagent Co. Ltd., China. Other reagents used in this work were purchased from Sinopharm Group Pharmaceutical Co. Ltd., China. All materials were used as received.

2.2. Hydroxylation

Every carbon paper with the size of 2.0×2.0 cm was refluxed in acetone at 65 °C for 2 h in order to remove impurities in it, rinsed with deionized water and dried. This purified carbon paper was denoted as untreated samples for comparison. The purified carbon paper was treated in a sealed 50 mL Teflon-lined stainless steel autoclave containing 40 mL mixed acid ($V_{H_2SO_4}/V_{HNO_3}$ = 3/1) solution for different time at 80 °C and under ultrasonication by using a temperature-adjustable sonicator (Bransonic 1510-DTH) with the maximum output of 70 W/42 kHz. The treated samples were washed with deionized water, sonicated in the deionized water at 80 °C for 0.5 h, rinsed again with deionized water until the pH of the rinsed water became neutral, and dried in vacuum oven at 60 °C for 8 h.

2.3. Characterization of hydroxylation

FTIR (Perkin-Elmer Spectrum RX-1, USA) were used to characterize the oxygen-containing groups on carbon fibres. 0.5 mg of the crashed carbon fibres were mixed with 40 mg of potassium bromide (KBr) to prepare a disk with 1.3 cm in diameter. This very low concentration is necessary due to the high absorption of the carbon fibres. Before the measurement, the disk was dried in vacuum oven at 60 °C for 8 h.

XPS spectra were obtained with ESCALAB250 XPS (Thermo Fisher Scientific, USA) at 2×10^{-9} mba. Al-Kα (1486.6 eV) was used as the X-ray source at 15 keV of anode voltage. The filament current and emission current were 4.6 A and 20 mA, respectively. Spectra were analyzed using Spectrum software (Xpspeak41).

TGA measurements were made using a TGA-7 thermal gravimetric analyzer (Perkin-Elmer, USA) from room temperature to 650 °C at the rate of 10 °C min^{-1}, under nitrogen atmosphere at the rate of 30 mL min^{-1}.

The surface morphology and structure of the samples were characterized with a scanning electron microscopy (JEOL, JSM-6380LV, Japan) at an acceleration voltage of 15 kV and an X-ray diffraction instrument (Rigaku D/MAX-RC, Japan) from 10° to 65°.

2.4. Characterization of electrochemical activity

For electrochemical measurement, a three-electrode cell was used with the carbon paper as the working electrode, a saturated calomel electrode (SCE) as the reference electrode and graphite plate as the counter electrode. The working electrode was prepared by sandwiching a piece of carbon paper sample into two plastic sheets. One sheet had an open of 0.739 cm^2 as the working area, and the other had a Ti plate that contacted the sample for current collecting. Cyclic voltammetry (CV) result was obtained with Multichannel Potentiostat (Solartron Analytical 1480 Multistat, England). Electrochemical impedance spectroscopy (EIS) was measured on Autolab workstation (PGSTAT-30, Netherlands) by applying an alternating voltage of 5 mV over the frequency ranging from 10^{-2} to 10^5 Hz. The solution for V(IV)/V(V) study consisted of 0.1 M V(IV) + 0.1 M V(V) + 3 M H_2SO_4, which was obtained by dissolving 4.6 g V_2O_5 and 10.6 g $VOSO_4{\cdot}3H_2O$ in the hot H_2SO_4 solution (The total volume is 500 mL, which contain 81 mL 98% concentrated sulfuric acid). The solution for V(II)/V(III) study consisted of 0.1 M V(II) + 0.1 M V(III) + 3 M H_2SO_4, which was obtained by mixing the equal volume 0.2 M V(II) + 3 M H_2SO_4 solution and 0.2 M V(III) + 3 M H_2SO_4 solution. Both of 0.2 M V(II) + 3 M H_2SO_4 solution and 0.2 M V(III) + 3 M H_2SO_4 solution were prepared by electro-reduction of 0.2 M V(IV) + 3 M H_2SO_4 solution. The complete reduction of V(IV) was confirmed by both the measurement of electrode potentials and UV–vis absorption spectra. The methods for the specific preparation of electrolyte solutions and the determination of vanadium concentration were used as those reported in references [5,27,28].

Constant current charge–discharge test was carried out by using a small-scale VRFB on a battery test system CT2001A (Wuhan Land Co., China). Two pieces of carbon papers with area of 4 cm^2 (2.0 × 2.0 cm) were served as positive and negative electrodes. The positive electrode compartment was separated from the negative electrode compartment with a Nafion 117 membrane (DuPont, USA) that was sealed with rubber washers. The initial catholyte was 1 M V(IV) + 3 M H_2SO_4, and the anolyte was 1 M V(III) + 3 M H_2SO_4, which were generated by electro-reduction of 1 M V(IV) + 3 M H_2SO_4 solution. The volume of both electrolytes was 10 mL.

3. Results and discussion

3.1. FTIR analysis

The functional groups of the untreated sample and the treated samples were characterized by FTIR and the results are shown in Fig. 1. In contrast to the untreated sample, the treated samples appear a wide absorption peak at 3450 cm^{-1}, which is characteristic of a stretching vibrational mode of —OH groups [29]. In addition, the vibrational band at 1615 cm^{-1} is characteristic of a stretching mode of —OH groups in the enol (C=C—OH) form [30]. These typical bands indicate that the —OH groups are introduced on the surface of carbon fibres after the treatment with mixed acids. The weaker peak at about 1755 cm^{-1} can be considered to be a trace of C=O groups in aldehyde, ketone or lactone groups [31].

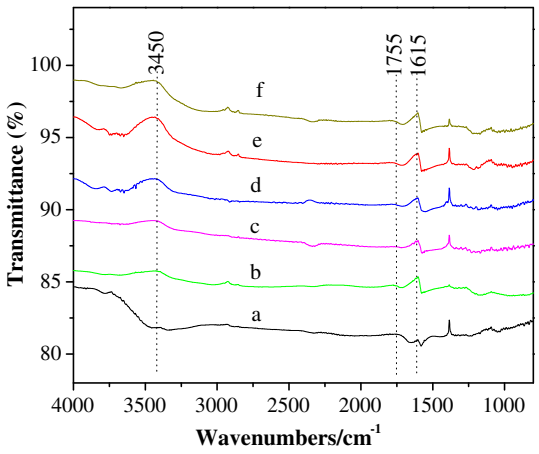

Fig. 1 – FTIR spectra of untreated carbon paper (a) and treated carbon papers in mixed acids ($V_{H_2SO_4}/V_{HNO_3}$ = 3/1) under ultrasonication for (b) 0.5, (c) 2, (d) 5, (e) 8, and (f) 10 h at 80 °C.

3.2. XPS analysis

Fig. 2 shows the XPS survey spectra of different samples. The spectra were calibrated against the major carbon peak at the binding energy of 284.7 eV. Fig. 3 presents the XPS analysis of C1s and O1s. The contents of surface elements and oxygen-containing groups of the samples can be obtained based on Figs. 2 and 3 and the results are listed in Table 1.

As shown in Fig. 2, with the increase of treatment time, the intensity of the O1s peak at the binding energy of 532 eV increases significantly with respect to that of the C1s peak at the binding energy of 284.7 eV. This indicates that the O content and O/C ratio increase for the samples, corresponding to the values shown in Table 1. It can be found from Table 1 that after the treatment for 10 h, the O content and O/C ratio reach 18.2% and 0.22, respectively, comparing to the 5.5% and 0.06 of the untreated sample.

As shown in Fig. 3, the carbon in C1s XPS has several electronic states. The main peak at 284.7 eV is attributed to graph-

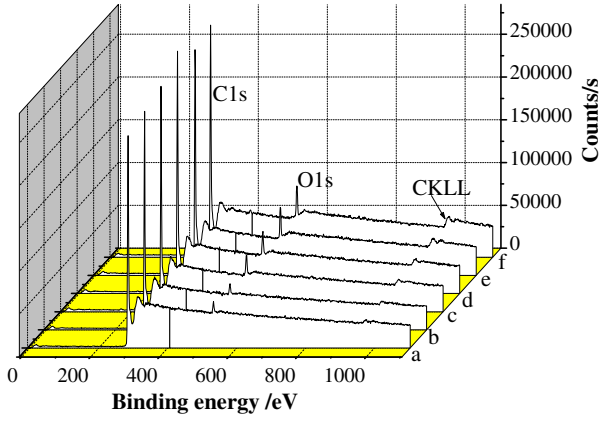

Fig. 2 – XPS survey spectra of untreated carbon paper (a), and treated carbon papers in mixed acids ($V_{H_2SO_4}/V_{HNO_3}$=3/1) under ultrasonication for (b) 0.5, (c) 2, (d) 5, (e) 8, and (f) 10 h at 80 °C.

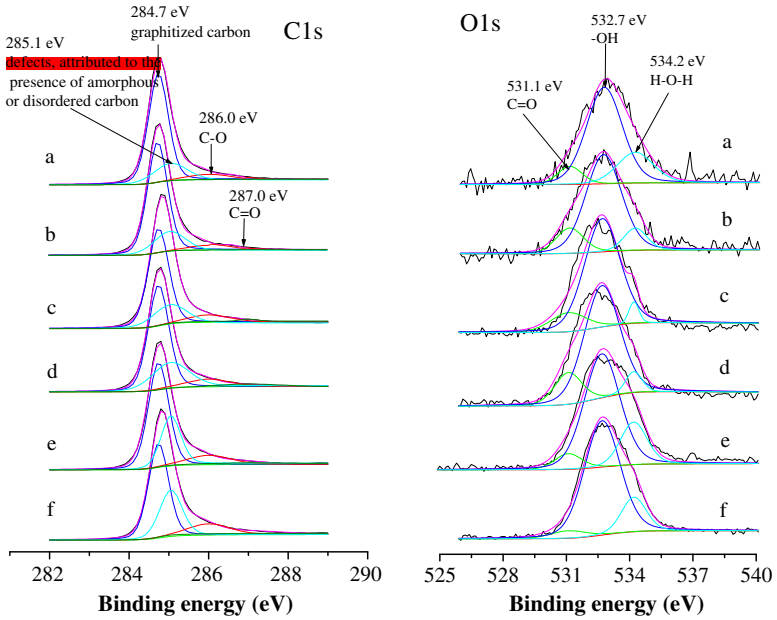

Fig. 3 – XPS C1s and O1s peaks of untreated carbon paper (a), and treated carbon papers in mixed acids ($V_{H_2SO_4}/V_{HNO_3}$ = 3/1) under ultrasonication for (b) 0.5, (c) 2, (d) 5, (e) 8, and (f) 10 h at 80 °C.

Table 1 – The contents of surface elements and oxygen-containing groups on the surface of carbon papers untreated and treated in mixed acids ($V_{H_2SO_4}/V_{HNO_3}$ = 3/1) under ultrasonication at 80 °C for different time.

Sample	Peak	Center	Area	O/C ratio	Graphitized carbon content $x_{A\,t}$%	O content $x_{A\,t}$%	O-H content $x_{A\,t}$%	H-O-H content $x_{A\,t}$%	C=O content $x_{A\,t}$%
Untreated	C_{1S}	284.77	54021.91	0.06	84.6	5.5	3.8	1.2	0.5
	O_{1S}	532.94	3165.76						
0.5 h	C_{1S}	284.78	50326.94	0.07	83.3	6.7	5.0	0.7	1.0
	O_{1S}	532.68	3622.03						
2 h	C_{1S}	284.84	53897.09	0.12	82.7	11.0	8.8	0.5	1.7
	O_{1S}	532.45	6675.05						
5 h	C_{1S}	284.78	56161.11	0.14	79.2	12.6	9.7	0.8	2.1
	O_{1S}	532.37	8081.44						
8 h	C_{1S}	284.78	53564.14	0.18	71.9	16.5	11.9	3.3	1.3
	O_{1S}	532.48	10583.51						
10 h	C_{1S}	284.83	54641.43	0.22	66.5	18.2	14.3	2.3	0.9
	O_{1S}	532.74	12185.04						

itized carbon (graphitic C=C and hydrocarbon C—C). The peak at 285.1 eV is attributed to defects on the carbon fibre structure [32]. The peak at 286.0 eV corresponds to the carbon in —OH groups (C—O) [33]. The weak peak at 287.0 eV is attributed to the carbon in C=O groups. The deconvolution of the C1s spectra (Fig. 3) reveals a decrease of the graphitic carbon layer accompanying with an increase of the defect peak with the increase of treatment time. It can be found that there is an apparent increase of —OH content with the increase of treatment time.

On the other hand, the O1s spectrum can be split to three peaks, which is consistent with the results of other authors [31,32]. The split peak located at 531.1 eV, 532.7 eV and 534.2 eV is corresponding to C=O, —OH and the adsorbed molecular water (H–O–H), respectively. Table 1 show a significant increase in the percentage content of —OH from 3.8% to 14.3% when the sample was treated for 10 h. The increased value of ca. 10% —OH corresponds to the density of ca. one —OH group per ten carbon atoms of carbon fibres, which is comparable to that of a solid-phase mechanochemical reaction treatment for SWCNT [17], and higher than that reported by Yang et al. [13], who treated multi-walled carbon nanotubes with a hydrothermal treatment in potassium hydroxide solution.

The formation of oxygen-containing groups on carbon material depends on its carbon source, microstructure and the treatment condition. The carbon paper is fabricated by the polyacrylonitrile through the wiredrawing, high-temperature carbonization and graphitization process. After these complicate processes, the microfibrillar of polyacrylonitrile-based carbon fibre can turn into the trapezoidal hexagonal ring-like lamellar structure [34]. The microfibrillar structure

can produce a lot of fragments such as alkane, cycloalkane, alkene, and dutrex, through the attack from the mixed acids during the treatment. The C=O groups mainly come from the further oxidization of —OH groups which result from the breakage of C=C bonds on the fragments under strong oxidation [35]. With the increase of treatment time in mixed acids, the content of C=O groups increases and reaches a maximum at 5 h, then decreases, as shown in Table 1. This phenomenon can be explained as follows. During the treatment initiation, only part of C=C bonds (the carbon atom of the surface edge) on the fragments are broken and the oxygen-containing groups consisting of mainly —OH formed on the carbons from the broken bonds. When the treatment proceeds for 5 h, almost all the C=C bonds on the fragments are broken and all the carbons from the broken bonds transform into —OH groups. At this moment, C=O group tends to be generated from the further oxidation of —OH. As the treatment proceeds further, C=O is further oxidized into carbon dioxide. On the other hand, the H_2SO_4 molecule can attack the defect sites, such as the unsaturated alkenes, conjugated double bonds and benzene ring, forming C—OSO_2OH which transforms to —OH when meeting H_2O [13,36,37]. The C—OSO_2OH groups also can protect the C=C from destroying. Therefore, when the treatment time is more than 5 h, the content of —OH groups increases again but the content of C=O groups decreases. Fig. 4 presents the involved reactions. The carbon in these defects should be more active than that in the hexagonal ring-like lamellar structure but the mechanism for the functionization should be similar for both carbons.

It can be seen from Table 1 that there is a decrease of water content on the fibre surface during first few hours of oxidation. This suggests that water molecules are not able to be absorbed onto the unpolar surface, which can be as a proof of the increase of hydrophility of the surface. As the treatment proceeds further, the increase of the —OH group content on the carbon fibre improves the polarity of its surface, which can be confirmed by the increased water content, as shown in Table 1. The change of the —OH group content on the carbon fibres surface is in agreement with that of the absorb water content, except for the case of the sample treated for 10 h, whose measured results might be affected by its deteriorated structure (see Fig. 6).

The treatment with mixed acids is more effective for the hydroxylation of carbon fibres than the treatment with sulfuric acid or nitric acid alone, because there is a synergetic effect in the treatment with mixed acids [16,38]. Nitric acid functions as an oxidant and sulfuric acid can accelerate the oxidation process of carbon by combining water generated during the oxidation. The mixed acids with H_2SO_4 and HNO_3 ($V_{H_2SO_4}/V_{HNO_3}$ = 3/1) are the most effective in the purification and oxidation process of the carbon nanotubes [39,40].

3.3. *Thermal stability*

Fig. 5 shows TGA curves of carbon papers treated in mixed acids for different time. It can be seen from Fig. 5 that, with the increase of treatment time, the weight loss of the sample becomes more and more significant. This should be ascribed to the release of oxygen-containing groups and a small amount of adsorbed water from the surface of the samples. The untreated sample remains thermally stable up to 650 °C, and the total weight loss is only 1.0% by mass. The treated samples show different TGA profiles from the untreated sample. The weight loss of the samples treated

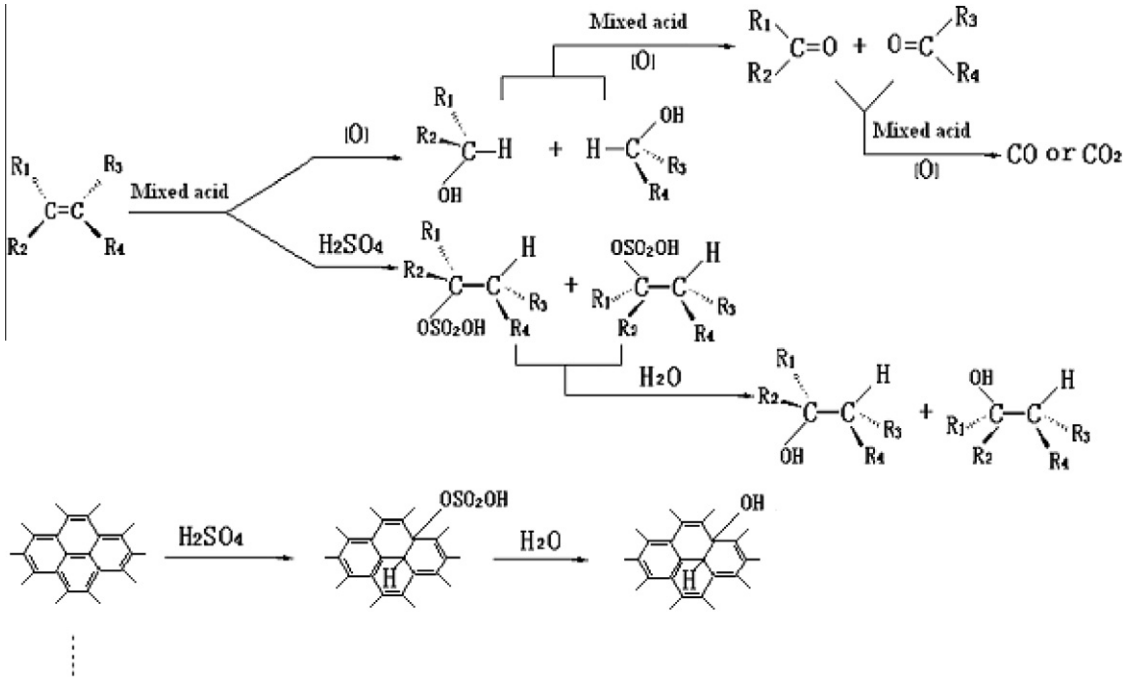

Fig. 4 – The possible reactions of carbon fibres in mixed acids ($V_{H_2SO_4}/V_{HNO_3}$=3/1) (R_1, R_2, R_3, R_4, R_5, R_6, and R_7 represent alkanes, cycloalkanes, alkenes, dutrex and other groups, respectively).

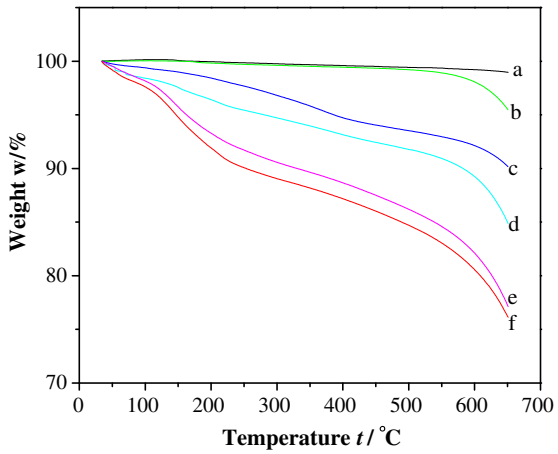

Fig. 5 – TGA curves of untreated carbon paper (a), and treated carbon papers in mixed acids ($V_{H_2SO_4}/V_{HNO_3}$ = 3/1) under ultrasonication for (b) 0.5, (c) 2, (d) 5, (e) 8, and (f) 10 h at 80 °C.

for 0.5, 2, 5, 8, and 10 h is 4.5%, 9.8%, 15.0%, 22.9%, and 24.0%, respectively. The tendency is consistent with the content of oxygen-containing groups on the surface of the samples.

3.4. SEM image

Fig. 6 shows the surface morphology of carbon paper samples. It can be seen that the surface of the carbon fibre in the untreated sample is smooth but becomes rough, and the rough degree increases with the increase of the —OH group content on the carbon fibres. This indicates that defect sites are introduced by the treatment. From the photo on top right corner of the Fig. 6f, it can be seen that the carbon paper is stratified, indicating that the mechanic strength and the surface of carbon paper were deteriorated when it was treated for 10 h. Therefore, the treatment for the hydroxylation of carbon paper with mixed acids should not last more than 8 h.

3.5. XRD pattern

Fig. 7 presents the XRD patterns of the different samples. The untreated sample exhibits several graphite peaks. The most significant peak is the (0 0 2) diffraction located at 26.4°. The weak peaks at about 42.4° and 54.3° correspond to (1 0 0) and (0 0 4) diffractions, respectively [41]. By comparing the XRD patterns of treated and untreated samples, it can be found that the treatment hardly changes the position but weakens the intensity of the diffraction peaks. This confirms the observation with SEM that more structural defects are introduced due to the treatment. These defects cause the par-

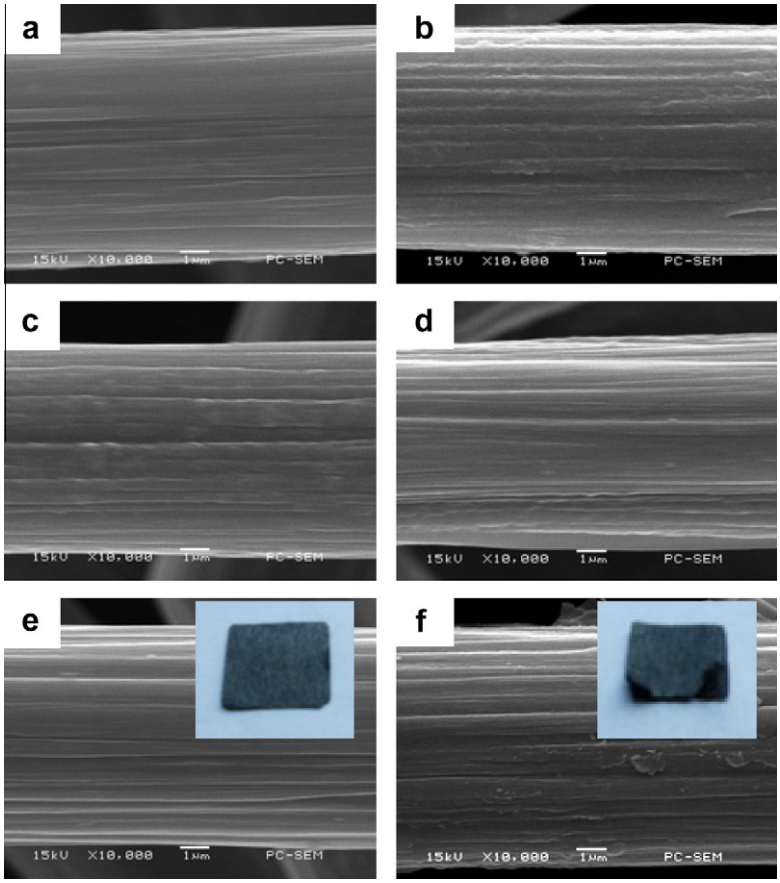

Fig. 6 – SEM images of untreated carbon paper (a), and treated carbon papers in mixed acids ($V_{H_2SO_4}/V_{HNO_3}$ = 3/1) under ultrasonication for (b) 0.5, (c) 2, (d) 5, (e) 8, and (f) 10 h at 80 °C.

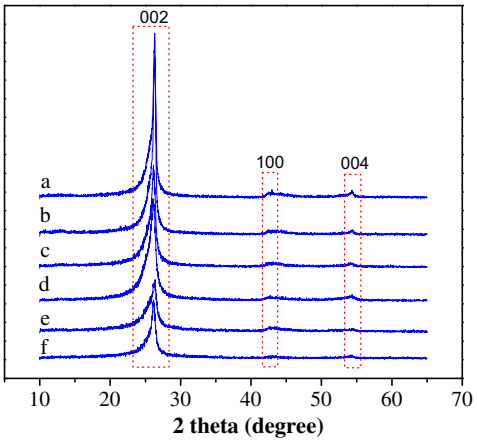

Fig. 7 – XRD patterns of untreated carbon paper (a), and treated carbon papers in mixed acids ($V_{H_2SO_4}/V_{HNO_3}$ = 3/1) under ultrasonication for (b) 0.5, (c) 2, (d) 5, (e) 8, and (f) 10 h at 80 °C.

tial disordering of in-plane reflection planes so that the corresponding diffraction peaks are weakened.

3.6. CV analysis

Fig. 8 presents the CV curves of V(IV)/V(V) and V(II)/V(III) redox couples on carbon paper electrodes (vs. SCE). The electrochemical parameters obtained from Fig. 8 are listed in Table 2. In Fig. 8A, the anodic peak O1 associated with the oxidation of V(IV) to V(V) and the corresponding reduction peak R1 appear at 1.0–1.2 V and 0.7–1.2 V (vs. SCE), respectively. Both oxidation peak current (I_{pa}) and reduction peak current (I_{pc}) increase with the increase of the —OH group content except for the sample treated for 10 h. Among all the samples, the sample treated for 8 h has the smallest peak potential separations (ΔE_p) and its ratio of oxidation peak current and reduction peak current (I_{pa}/I_{pc}) is close to 1, indicating that the sample treated for 8 h exhibits the best electrochemical activity for V(IV)/V(V) redox reaction.

Table 2 – The parameters obtained from the CV curves for V(IV)/V(V) on the carbon paper electrodes untreated and treated for different time in mixed acids ($V_{H_2SO_4}/V_{HNO_3}$ = 3/1).

Sample	E_{pa} (V)	E_{pc} (V)	I_{pa} (mA)	I_{pc} (mA)	$\triangle E_p$ (V)	I_{pa}/I_{pc}
Untreated	1.07	0.72	7.06	3.82	0.35	1.85
0.5 h	1.09	0.70	8.67	5.00	0.39	1.73
2 h	1.08	0.71	15.19	12.66	0.37	1.20
5 h	1.06	0.71	16.79	15.72	0.35	1.07
8 h	0.99	0.77	24.03	22.79	0.22	1.05
10 h	1.02	0.75	23.32	22.10	0.27	1.06

The mechanism on the improved activity of carbon fibres toward V(IV)/V(V) redox reaction by —OH groups can be given in Fig. 9. It involves the transport of vanadium ions (V(IV) or V(V) ions) from the bulk of the solution to the electrode surface, their ion-exchange with hydrogen ions in the —OH groups on carbon and the succeeding electron transfer reaction [41]. The larger reaction current of the treated samples is ascribed to their higher surface vanadium ion concentration which results from the higher —OH content on carbon. Thus, the sample with higher surface concentration of —OH groups exhibits higher activity toward V(IV)/V(V) redox reaction. The sample treated for 10 h has higher —OH group contents but exhibits poorer activity than the sample treated for 8 h, because the deteriorated mechanical property of the sample treated for 10 h reduces the effective area for V(IV)/V(V) redox reaction.

Fig. 8B shows the CV curves of V(II)/V(III) on the different samples. The oxidation peaks O2 associated with the oxidation of V(II) to V(III) and the corresponding reduction peaks appear R2 at −0.3 to −0.4 V and −0.6 to −0.8 V (vs. SCE), respectively. Similar to the V(IV)/V(V) redox reaction, the sample treated for 8 h exhibits the best electrocatalytic activity toward V(II)/V(III) redox reaction. It should be noted that different from the behavior for V(IV)/V(V) redox reaction, the untreated sample does not show its activity toward V(II)/V(III) redox reaction. The treated samples show high electrocatalytic activity toward V(II)/V(III) redox reaction, as

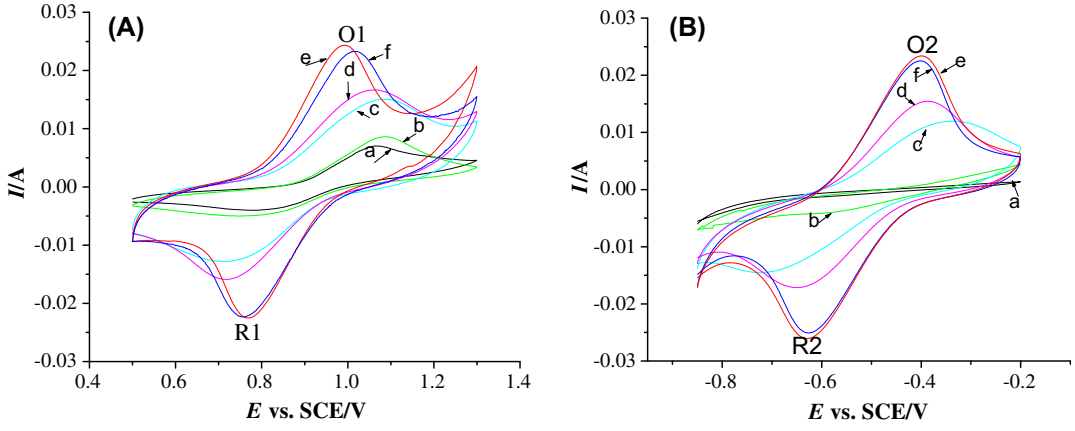

Fig. 8 – CV curves recorded at 0.01 V·s^{-1} in (A) 0.1 M V(IV) + 0.1 M V(V) + 3 M H_2SO_4 solution and (B) 0.1 M V(II) + 0.1 M V(III) + 3 M H_2SO_4 solution at untreated carbon paper electrode (a), and treated carbon papers in mixed acids ($V_{H_2SO_4}/V_{HNO_3}$ = 3/1) under ultrasonication at 80 °C for (b) 0.5, (c) 2, (d) 5, (e) 8, and (f) 10 h.

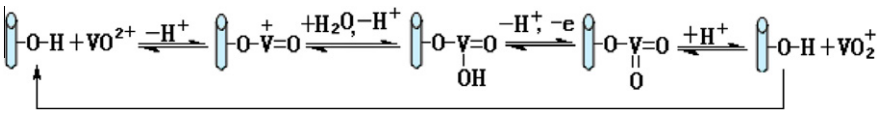

Fig. 9 – The mechanism on the improved activity of carbon fibres toward V(IV)/V(V) redox reaction by —OH groups.

seen from Fig. 8B, suggesting that the V(II)/V(III) redox reaction more strongly depends on the —OH groups on the carbon fibres than the V(IV)/V(V) redox reaction. This may be attributed to the different forms of vanadium ions in sulfuric solution. V(IV) and V(V) exist in the form of ions containing oxygen but V(II) and V(III) ions are more simple [3]. Thus, the V(IV) and V(V) ions are more easy to proceed with the ion-exchange reactions with hydrogen ions in the —OH groups than the V(II) and V(III) ions, resulting in the different dependence of the reaction activity on the —OH groups on the carbon fibres. The mechanism on the improved activity of carbon fibres toward the V(II)/V(III) redox reaction by —OH groups can be expressed in Fig. 10.

3.7. *EIS analysis*

Fig. 11 displays the Nyquist plots of carbon paper electrodes in 0.1 M V(IV) + 0.1 M V(V) + 3 M H_2SO_4 solution at the open-circuit potential. It can be seen from Fig. 11 that the Nyquist plots include a semicircle part and a linear part, indicating that the V(IV)/V(V) redox reaction is mix-controlled by charge transfer and diffusion steps. The semicircle part at high frequencies reflects the charge transfer process and the linear part at low frequencies reflects the diffusion processes in pore channel of carbon paper [42–45]. Thus, the Nyquist plots can be fitted with the equivalent circuit of Fig. 12. In the equivalent circuit, R_1 stands for the resistance composed of solution resistance (R_s) and electrode resistance (R_e), R_2 represents the charge transfer resistance across electrode/solution interface (R_{ct}), CPE_1 is the constant-phase element which represents the electric double-layer capacitance of electrode/solution interface, and CPE_2 is the constant-phase element which represents the diffusion capacitance attributed by the diffusion process of V(IV) and V(V) ions in pore channel of the carbon paper electrodes [46]. The fitting results (solid lines in Fig. 11) reveal that this equivalent circuit can explain the electrochemical process on the carbon paper electrodes.

Table 3 lists the parameters obtained from fitting the impedance plots of Fig. 11 with the equivalent circuit of Fig. 12. It can be seen from Table 3 that there is not significant changes in R_1 for each sample, indicating that the treatment hardly influences the electronic conductivity of carbon papers. However, the charge transfer resistance R_2 depends on the treatment time. The charge transfer resistance decreases with increase of the treatment time except for the sample treated for 10 h. From the Table 3, it can seen that $Y_{0,1}$ and $Y_{0,2}$ increase with the increase of the content of —OH groups on the carbon papers except for the sample treated for 10 h, indicating that hydroxylation treatment enhances the electric double-layer capacitance of electrode/solution interface and the diffusion capacitance of ions in pore channel. The former favors the charge transfer for the V(IV)/V(V) redox reaction

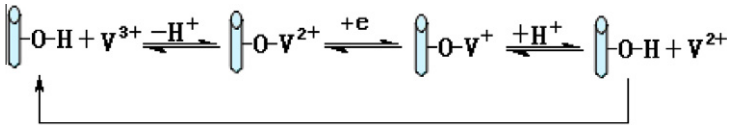

Fig. 10 – The mechanism on the improved activity of carbon fibres toward V(II)/V(III) redox reaction by —OH groups.

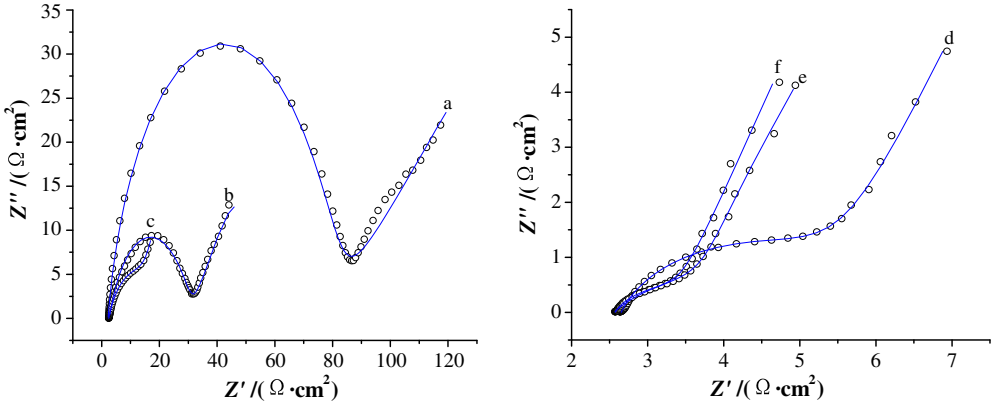

Fig. 11 – Nyquist plots of different carbon paper electrodes in 0.1 M V(IV) + 0.1 M V(V) + 3 M H_2SO_4 solution at open-circuit potential. Untreated carbon paper (a) and treated carbon paper in mixed acids ($V_{H_2SO_4}/V_{HNO_3}$ = 3/1) under ultrasonication for (b) 0.5, (c) 2, (d) 5, (e) 8, and (f) 10 h at 80 °C. The dots are the experimental results and the solid lines are the results from fitting by the equivalent circuits in Fig. 12.

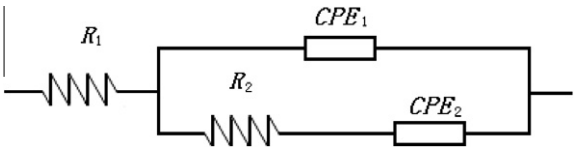

Fig. 12 – Equivalent circuit for the electrode process mix-controlled by charge transfer and diffusion steps.

and the latter favors the diffusion of V(IV) and V(V) ions within the pore channels in electrode.

The electrochemical impedance plots of carbon paper electrodes in 0.1 M V(II) + 0.1 M V(III) + 3 M H_2SO_4 solution at open-circuit voltage are also obtained. The results are shown in Fig. 13. The Nyquist plots of the electrodes in 0.1 M V(II) + 0.1 M V(III) + 3 M H_2SO_4 solution are similar to those in 0.1 M V(IV) + 0.1 M V(V) + 3 M H_2SO_4 solution, indicating that the electrode process is also mix-controlled by charge transfer and diffusion of V(II) and V(III) ions in the pore channel of the electrode. The parameters obtained from the fitting with the equivalent circuit of Fig. 12 are listed in Table 4. It can be seen that the dependence of charge transfer resistance of the V(II)/V(III) redox reaction on the treatment time is similar to that of the V(IV)/V(V) redox reaction. Each electrode has larger charge transfer resistance for V(II)/V(III) redox reaction, compared with V(IV)/V(V) redox reaction, which is in agreement with the difference in current of CV between two electrodes.

Table 3 – Parameters obtained from fitting the impedance plots of Fig. 11 with the equivalent circuit of Fig. 12.

Sample	R_1 (Ω cm^2)	CPE_1		R_2 (Ω cm^2)	CPE_2	
		$Y_{0,1}$	n_1		$Y_{0,2}$	n_2
Untreated	2.52	0.62×10^{-4}	0.85	76.61	0.54×10^{-1}	0.33
0.5 h	2.58	0.49×10^{-3}	0.73	28.02	0.20	0.48
2 h	2.46	0.95×10^{-1}	0.66	12.23	0.92	0.76
5 h	2.65	0.17	0.79	3.28	1.50	0.79
8 h	2.57	0.57	0.62	1.26	1.70	0.92
10 h	2.56	0.51	0.58	2.29	1.50	0.90

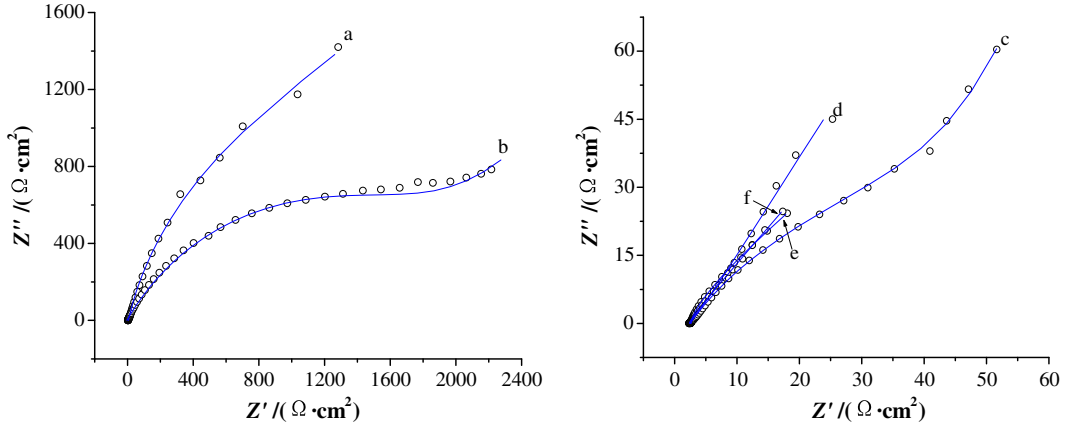

Fig. 13 – Nyquist plots of different carbon paper electrodes in 0.1 M V(II) + 0.1 M V(III) + 3 M H_2SO_4 solution at open-circuit potential. Untreated carbon paper (a) and treated carbon papers in mixed acids ($V_{H_2SO_4}/V_{HNO_3}$ = 3/1) under ultrasonication for (b) 0.5, (c) 2, (d) 5, (e) 8, and (f) 10 h at 80 °C. The dots are the experimental results and the solid lines are the results from fitting by the equivalent circuits in Fig. 12.

Table 4 – Parameters obtained from fitting the impedance plots of Fig. 13 with the equivalent circuit of Fig. 12.

Sample	R_1 (Ω cm^2)	CPE_1		R_2 (Ω cm^2)	CPE_2	
		$Y_{0,1}$	n_1		$Y_{0,2}$	n_2
Untreated	2.50	0.32×10^{-3}	0.84	2.49×10^{3}	0.42×10^{-2}	0.61
0.5 h	2.47	0.39×10^{-2}	0.62	2.22×10^{3}	0.60×10^{-2}	0.58
2 h	2.51	0.46×10^{-1}	0.70	105.50	0.13×10^{-1}	0.71
5 h	2.46	0.80×10^{-1}	0.86	5.21	0.86×10^{-1}	0.67
8 h	2.53	0.21	0.96	4.96	0.11	0.60
10 h	2.57	0.18	0.78	7.96	0.10	0.56

3.8. Charge–discharge test

Charge–discharge experiments are performed by using the small-scale cell with the carbon paper electrodes, in which, 10 mL 1 M V(IV) + 3 M H_2SO_4 and 10 mL 1 M V(III) + 3 M H_2SO_4 solutions are pumped into the positive and negative chamber as catholyte and anolyte, respectively. Fig. 14 presents the 50th charge–discharge curves of the cells at the current density of 10 mA cm^{-2}. It can be seen from Fig. 14 that the cell using the untreated sample has a very low capacity and the capacity of the cells using the treated samples are improved. The capacity of the cells increases with the increase of the treatment time except for the cell using the sample treated for 10 h, which are related to the activity of the samples toward two electrode reactions.

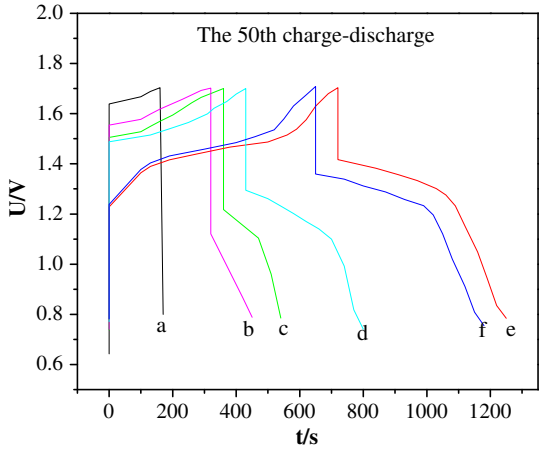

Fig. 14 – The 50th charge–discharge curves of the cells using different carbon paper electrodes at a current density of 10 mA cm^{-2}. Untreated carbon paper (a) and treated carbon papers in mixed acids ($V_{H_2SO_4}/V_{HNO_3}$ = 3/1) under ultrasonication for (b) 0.5, (c) 2, (d) 5, (e) 8, and (f) 10 h at 80 °C.

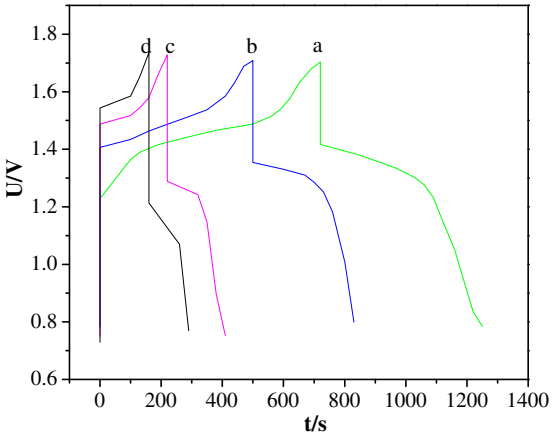

Fig. 15 – Charge–discharge curves of the cell using the carbon paper electrodes treated in mixed acids ($V_{H_2SO_4}/V_{HNO_3}$ = 3/1) under ultrasonication for 8 h at 80 °C at the rate of (a) 10, (b) 20, (c) 30, and (d) 40 mA cm^{-2}.

Table 5 – VRFB efficiencies of the cell using the carbon paper electrodes treated in mixed acids ($V_{H_2SO_4}/V_{HNO_3}$ = 3/1) under ultrasonication at 80 °C for 8 h at different charge–discharge rates.

Current density (mA cm^{-2})	Cycle number	Cell efficiency(%) [a]		
		η_C	η_V	η_E
10	1	78.3	91.1	71.3
	50	83.2	91.5	76.1
	100	80.3	91.6	73.6
20	1	83.6	86.3	72.2
	50	83.9	86.4	72.5
	100	85.4	85.8	73.3
30	1	86.5	81.8	70.7
	50	86.3	81.9	70.7
	100	86.6	81.8	70.8
40	1	87.6	72.5	63.5
	50	90.7	72.1	65.4
	100	87.6	71.4	62.5

a η_C, coulombic efficiency; η_V, voltage efficiency; η_E, energy efficiency.

Fig. 15 presents the typical charge–discharge curves of the cell using the carbon paper sample treated for 8 h at the rate of 10, 20, 30, and 40 mA cm^{-2}. It can be found that the cell maintains high charge–discharge performance under different rates. The average coulombic, voltage and energy efficiencies of the cell are listed in Table 5. It can be seen from Table 5 that the cell succeeds in maintaining almost cell efficiencies at different charge–discharge rates. Even when the charge–discharge rate is 40 mA cm^{-2}, the coulombic, voltage and energy efficiencies reach as high as 87.6%, 71.4%, and 62.5%, respectively. The highest energy efficiency of the cell could be obtained was 76.1% at 10 mA cm^{-2}. The average energy efficiencies at all kinds of charge–discharge rates in this work are all higher than the results reported by Wang et al. [40], who used both the Ir-modified and thermal-modified carbon felt electrodes in the VRFB.

4. Conclusions

Carbon paper made from carbon fibres can be successfully hydroxylated by the treatment using mixed acids ($V_{H_2SO_4}/V_{HNO_3}$ = 3/1). The content of —OH groups on the carbon fibres increases with increase of the treatment time. However, due to the seriously damaged surface, the most highly hydroxylated sample treated for 10 h does not show highest activity toward the redox reactions of V(II)/V(III) and V(IV)/V(V). The VRFB using the carbon paper treated for 8 h as the positive and negative electrodes exhibits excellent performance under a current density of 10 mA cm^{-2}. The average voltage efficiency reaches 91.3%, and the corresponding average energy efficiency is 75.1%.

Acknowledgment

This work was supported by the national 863 project (Grant No. 2009AA05Z112).

REFERENCES

[1] Skyllas-Kazacos M, Rychcik M, Robins RG, Fane AG. New all-vanadium redox flow cell. J Electrochem Soc 1986;133(5):1057–8.

[2] Kaneko H, Nozaki K, Wada Y, Aoki T, Negishi A, Kamimoto M. Vanadium redox reactions and carbon electrodes for vanadium redox flow battery. Electrochem Acta 1991;36(7):1191–6.

[3] Gattrell M, Park J, MacDougall B, Apte J, McCarthy S, Wu CW. Study of the mechanism of the vanadium 4+/5+ redox reaction in acidic solutions. J Electrochem Soc 2004;151(1):123–30.

[4] Zhu HQ, Zhang YM, Yue L, Li WS, Li GL, Shu D, et al. Graphite–carbon nanotube composite electrodes for all vanadium redox flow battery. J Power Sources 2008;184(2):637–40.

[5] Oriji G, Katayama Y, Miura T. Investigations on V(IV)/V(V) and V(II)/V(III) redox reactions by various electrochemical methods. J Power Sources 2005;139(1–2):321–4.

[6] Rychcik M, Skyllas-Kazacos M. Characteristics of a new all-vanadium redox flow battery. J Power Sources 1988;22(1):59–67.

[7] Kamarudin SK, Daud WRW, Ho SL, Hasran UA. Overview on the challenges and developments of micro-direct methanol fuel cells (DMFC). J Power Sources 2007;163(2):743–54.

[8] Fabjan C, Garche J, Harrer B, Jorissen L, Kolbeck C, Philippi F, et al. The vanadium redox-battery: an efficient storage unit for photovoltaic systems. Electrochem Acta 2001;47(5):825–31.

[9] Zhou CF, Kumar S, Doyle CD. Functionalized single wall carbon nanotubes treated with pyrrole for electrochemical supercapacitor membranes. Chem Mater 2005;17(8):1997–2002.

[10] Tseng CH, Wang CC, Chen CY. Functionalizing carbon nanotubes by plasma modification for the preparation of covalent-integrated epoxy composites. Chem Mater 2007;19(2):308–15.

[11] Shen WZ, Wang H, Guan RG, Li ZJ. Surface modification of activated carbon fiber and its adsorption for vitamin B1 and folic acid. Colloids Surf A: Physicochem Eng Aspects 2008;331(3):263–7.

[12] Zhao P, Zhang HM, Zhou HT, Yi BL. Nickel foam and carbon felt applications for sodium polysulfide/bromine redox flow battery electrodes. Electrochim Acta 2005;51(6): 1091–8.

[13] Yang D, Guo GQ, Hu JH, Wang CC, Jiang DL. Hydrothermal treatment to prepare hydroxyl group modified multi-walled carbon nanotubes. J Mater Chem 2008;18(3):350–4.

[14] Kang ZH, Wang EB, Mao BD, Su ZM, Gao L, Niu L, et al. Heterogeneous hydroxylation catalyzed by multi-walled carbon nanotubes at low temperature. Appl Catal A 2006;299:212–7.

[15] Chen SM, Wu GZ, Chen DY. An easy approach to hydroxyethylated SWNTs and the high thermal stability of the inner grafted hydroxyethyl groups. Nanotechnology 2006;17(9):2368–72.

[16] Tian R, Wang XB, Li MJ, Hu HT, Chen R, Liu FM, et al. An efficient route to functionalize single-walled carbon nanotubes using alcohols. Appl Surf Sci 2008;255(5):3294–9.

[17] Pan HL, Liu LQ, Guo ZX, Dai LM, Zhang FS, Zhu DB, et al. Carbon nanotubes from mechanochemical reaction. Nano Lett 2003;3(1):29–32.

[18] Marshall MW, Popa-Nita S, Shapter JG. Measurement of functionalised carbon nanotube carboxylic acid groups using a simple chemical process. Carbon 2006;44(7):1137–41.

[19] Zhou JH, Sui ZJ, Zhu J, Li P, Chen D, Dai YC, et al. Characterization of surface oxygen complexes on carbon nanofibers by TPD, XPS and FT-IR. Carbon 2007;45(4):785–96.

[20] Paiva MC, Bernardo CA, Nardin M. Mechanical, surface and interfacial characterisation of pitch and PAN-based carbon fibres. Carbon 2000;38(9):1323–38.

[21] Wang YQ, Viswanathan H, Audi AA, Sherwood PMA. X-ray photoelectron spectroscopic studies of carbon fiber surfaces. 22. Comparison between surface treatment of untreated and previously surface-treated fibers. Chem Mater 2000;12(4):1100–7.

[22] Wu ZH, Pittman Jr CU, Gardner SD. Nitric acid oxidation of carbon fibers and the effects of subsequent treatment in refluxing aqueous NaOH. Carbon 1995;33(5):597–605.

[23] Pittman Jr CU, He GR, Wu B, Gardner SD. Chemical modification of carbon fiber surfaces by nitric acid oxidation followed by reaction with tetraethylenepentamine. Carbon 1997;35(3):317–31.

[24] Sun B, Skyllas-Kazacos M. Modification of graphite electrode materials for vanadium redox flow battery application – part II: acid treatment. Electrochim Acta 1992;37(7):2459–65.

[25] Laachachi A, Vivet A, Nouet G, Doudou BB, Poilâne C, Chen J, et al. A chemical method to graft carbon nanotubes onto a carbon fiber. Mater Lett 2008;62(3):394–7.

[26] Rasheed Asif, Howe JY, Dadmun MD, Britt PF. The efficiency of the oxidation of carbon nanofibers with various oxidizing agents. Carbon 2007;45(5):1072–80.

[27] Kazacos M, Cheng M, Skyllas-Kazacos M. Vanadium redox cell electrolyte optimization studies. J Appl Electrochem 1990;20(3):463–7.

[28] Kausar N, Howe R, Skyllas-Kazacos M. Raman spectroscopy studies of concentrated vanadium redox battery positive electrolytes. J Appl Electrochem 2001;31(12):1327–32.

[29] Osorio AG, Silveira ICL, Bueno VL, Bergmann CP. H_2SO_4/HNO_3/HCl – functionalization and its effect on dispersion of carbon nanotubes in aqueous media. Appl Surf Sci 2008;255(5):2485–9.

[30] Mawhinney DB, Naumenko V, Kuznetsova A, Yates JT, Liu J, Smalley RE. Infrared spectral evidence for the etching of carbon nanotubes: ozone oxidation at 298 K. J Am Chem Soc 2000;122(10):2383–4.

[31] Raghuveer MS, Agrawal S, Bishop N, Ramanath G. Microwave-assisted single-step functionalization and in situ derivatization of carbon nanotubes with gold nanoparticles. Chem Mater 2006;18(6):1390–3.

[32] Kim YJ, Lee HJ, Lee SW, Cho BW, Park CR. Effects of sulfuric acid treatment on the microstructure and electrochemical performance of a polyacrylonitrile (PAN)-based carbon anode. Carbon 2005;43(1):163–9.

[33] Datsyuk V, Kalyva M, Papagelis K, Parthenios J, Tasis D, Siokou A, et al. Chemical oxidation of multiwalled carbon nanotubes. Carbon 2008;46(6):833–40.

[34] Tokarsky EW, Diefendorf RG. Relationships beween three-dimensional structure models and properties in carbon fibres. Carbon 1973;11(6):691.

[35] Mawhinney DB, Naumenko V, Kuznetsova A, Yates JT, Liu J, Smalley RE. Surface defect site density on single walled carbon nanotubes by titration. Chem Phys Lett 2000;324(1–3): 213–6.

[36] Kakade BA, Pillai VK. An efficient route towards the covalent functionalization of single walled carbon nanotubes. Appl Surf Sci 2008;254(16):4936–43.

[37] Valdés H, Zaror CA. Ozonation of benzothiazole saturated-activated carbons: influence of carbon chemical surface properties. J Hazard Mater 2006;137(2):1042–8.

[38] MacKenzie K, Dunens O, Harris AT. A review of carbon nanotube purification by microwave assisted acid digestion. Sep Purif Technol 2009;66(2):209–22.

[39] Goyanes S, Rubiolo GR, Salazar A, Jimeno A, Corcuera MA, Mondragon I. Carboxylation treatment of multiwalled carbon nanotubes monitored by infrared and ultraviolet spectroscopies and scanning probe microscopy. Diamond Relat Mater 2007;16(2):412–7.
[40] Lee G-W, Kim J, Yoon J, Bae J-S, Shin BC, Kim IS, et al. Structural characterization of carboxylated multi-walled carbon nanotubes. Thin Solid Films 2008;516(17):5781–4.
[41] Sun B, Skyllas-Kazacos M. Modification of graphite electrode materials for vanadium redox flow battery application – I: thermal treatment. Electrochem Acta 1992;37(7):1253–60.
[42] Wang WH, Wang XD. Investigation of Ir-modified carbon felt as the positive electrode of an all-vanadium redox flow battery. Electrochim Acta 2007;52(24):6755–62.
[43] Meyers JP, Doyle M, Darling RM, Newman J. The impedance response of a porous electrode composed of intercalation particles. J Electrochem Soc 2000;147(8):2930–40.
[44] Albery WJ, Mount AR. The ac impedance of a three-ion thin layer cell. J Electroanal Chem 1992;325(1–2):95–110.
[45] Xiao P, Gao WY, Qiu XP, Zhu WT, Sun J, Chen LQ. Thermal behaviors of Ni-MH batteries using a novel impedance spectroscopy. J Power Sources 2008;182(1):377–82.
[46] Oriji G, Katayama Y, Miura T. Investigation on V(IV)/V(V) species in a vanadium redox flow battery. Electrochim Acta 2004;49(19):3091–5.